

Supporting Information

Ferroelectric-like Organic-Inorganic Interfaces

*Linlin Yang, Jianxin Guo, Jian Li, Jun Yan, Kunpeng Ge, Jiayue Jiang, Han Li, Benjamin S. Flavel, Baoting Liu, and Jianhui Chen**

*Correspondence to: chenjianhui@hbu.edu.cn (J. Chen).

Experimental Section

Thin Film and Device Fabrication

Si wafers were first dipped into 5% hydrofluoric acid (HF) to remove the native oxide layer, which resulted in a H-terminated Si surface with Si-H bonds and dangling bond defects. Poly(4-styrenesulfonic acid) (PSS) thin films were spin-coated onto silicon from a precursor solution (Sigma Aldrich, 18 wt. % in H₂O) at 3500–7500 rpm in ambient atmosphere and subsequently annealed at 100 °C for 10 min under a vacuum of 0.1–1 Pa. The film thickness was controlled by adjusting the solution concentration and rotation speed. p-type (100)-oriented FZ silicon wafers with a resistivity of 1–5 Ω•cm and a thickness of 280 μm were obtained from GlobalWafers Co., Ltd. Circular parallel plate capacitors were constructed by evaporating a 200 nm top Ag layer through a shadow-mask with a pad diameter of 400 μm.

Fabrication of Black-Silicon

Si nanowire arrays were fabricated via a metal-assisted chemical etching technique [1]. Si wafers were coated with a Ag nanoparticle film by electroless metal deposition method in an aqueous solution of 6 ml 10 % HF (Tianjin Kemiou Chemical Reagent Co., China), 0.2 g AgNO₃, and 240 ml deionized water for 5 minutes. The metal-treated Si wafers were immersed in HF-based aqueous chemical etching solutions 43 ml 10 % HF, 3.8 ml 30 % H₂O₂, (Tianjin Kemiou Chemical Reagent Co., China) and 153 ml deionized water at different etching times to obtain Si nanowires of various lengths. After nanowire formation the wafers were dipped into the aqueous solution of 40 ml 25-28 % NH₄OH, (Tianjin Kemiou Chemical Reagent Co., China) 40 ml H₂O₂, and 200 ml deionized water for 5 min for removing residual Ag nanoparticles. After treatment, the as-synthesized Si nanowire arrays were rinsed with deionized water and dried at room temperature using N₂.

Materials and Device Characterization

The ferroelectric behavior (hysteresis loops, fatigue, and retention) of the parallel plate capacitors were measured using a ferroelectric tester (Radiant Technologies, Precision Multiferroic II and Ferroelectric Test System). The hysteresis loop was measured under a standard bipolar drive profile at an optimized frequency of 10 kHz. The fatigue behavior of the capacitor was tested under asquare drive signal with a peak voltage of 4 V and a frequency of 10 kHz, in which this waveform voltage was applied for 1/2 of the waveform period and the negative of the voltage was applied for the other 1/2 of the period. The retention experiment was performed using a direct descendent of the popular Retain Programs provided with the Radiant Technologies RT66A and RT6000 series testers. The structure of the PSS thin film was characterized by X-ray diffraction (XRD) (TD-3700). For the study of the interface state switching, the interface recombination velocity was measured with a Sinton WCT-120 instrument using a technique based on photoconductance measurements. In this measurement, samples as large as 4 cm × 4 cm were fabricated to match the inductive coil, and a transparent conductive electrode, indium tin oxide (ITO), was used to ensure transparency to light. The interface properties of as-prepared, before poling and after poling samples were investigated by high-resolution transmission electron microscopy (HRTEM) (Tecnai G2 F20 S-Twin). The photoluminescence (PL) measurements under positive and

negative poling voltages were performed using an ITO/PSS/Si/PSS/ITO sample geometry. The leakage current of the capacitor was measured by Keithley 2601B Source Meter instruments.

Interface HRTEM Characterization

Prior to preparing cross-sectional TEM specimens, the samples needed to be polarized. The structure of the sample was ITO and/or Ag/PSS/Si. On one side of the Si wafer, most of the area was covered by ITO/PSS. One sample was marked as as-prepared without any electrical processing. The P_r-up specimen was biased at 1.5 V with ITO as a positive electrode and Ag as a negative electrode. Oppositely, the P_r-down sample was biased at 2 V with ITO as a negative electrode and Ag as a positive electrode. The Focused Ion Beam (FIB) thinning technique was used to prepare the samples for TEM. Due to the solubility of PSS in H₂O, acetone, and alcohol, it was difficult to prepare TEM samples using other thinning techniques, such as mechanical milling or manual polishing method. Using the FIB technique, the specimen can be thinned in a precise thickness, on the nanometric scale. It first a Pt layer was deposited to protect the surface during ion milling, and then using a Ga³⁺ ion beam to machine two parallel trenches on both sides of the sample area to be observed, the resulting wall constituted the parallel-sided thin slice. Using the internal micromanipulator to extract the sample after final thinning and then taken out of the FIB to be observed in the TEM.

Density Function Theory (DFT) Calculations

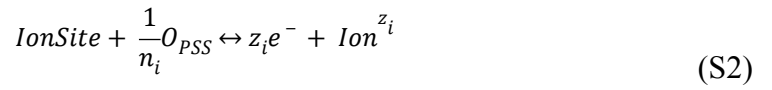
Structural optimizations were performed with the Vienna ab initio Simulation Package (VASP) code [2,3] based on DFT. For the exchange and correlation energy, the Perdue-Burke-Ernzerhof (PBE) function [4] under the generalized gradient approximation (GGA) was employed. The ion-electron interaction was treated by the projector augmented wave (PAW) method [5]. A cut-off energy of 500 eV for plane-wave basis set and a 4×4×1 Monkhorst-Pack k-mesh for Brillouin-zone integration was used for a 2×2 super-cell structural relaxation with fixing under ten layers. The Methfessel-Paxton smearing scheme [6] with the smearing width of 0.1 eV was applied to the Brillouin-zone integrations and the magnitude of the force acting on each atom became less than 0.005 eV/Å. The conjugate gradient method and the total energy of the optimized structures were well-converged (10⁻⁶ eV per cell). The van der Waals (vdW) interaction in Si-PSS system is included using a dispersion correction term with DFT-D3 method [7,8]. A large vacuum space of 25 Å was used for avoid any interaction between sheets. The adsorption model for the PSS/Si interface consists of the H-terminated Si (001) surface with dangling bonds and the corresponding PSS single molecule adsorption system. The PSS monomer molecule was selected as the simple model of PSS to decrease computational complexity. In reality a well ordered and crystalline layer of PSS will not be formed at the Si interface and DFT structural optimizations are only employed to reveal the possibility of two interfacial configurations which correspond to chemically bound and unbound PSS at the silicon surface. To describe the chemisorption of PSS on the Si-H (001) surface, the adsorption energy was defined as:

$$E_{Adsorption} = E_{Total} - E_{Si-H} - E_{PSS} \quad (S1)$$

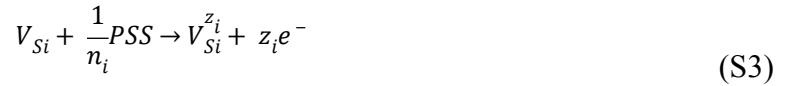
where $E_{Adsorption}$ is defined as the total energy (E_{Total}) minus the energy of the individual components (E_{Si-H} and E_{PSS}). A negative $E_{Adsorption}$ indicates the stability of the adsorption structures.

Stephenson & Highland Calculation of Mixed Electrochemical-Ferroelectric Systems.

For a mixed electrochemical-ferroelectric system the polarization (P) is related to the surface charge density (σ) at the Si:PSS interface, such that $P \approx -\sigma$ [9]. This is a property that is defined by the number of the Si–O bonds at the interface and will vary with the applied voltage. Stephenson and Highland define a generalized electrochemical equation [9] to describe this process



In this work the transition between bound and unbound PSS states can be described by the two half equations:



Where the notation O and V stand for silicon states occupied (O) with- and vacant (V) of PSS, n_i is the number of surface ions (Si–O) created per PSS molecule (two bound oxygen atoms), z_i is the charge of the surface ion. n_i and z_i are positive or negative depending on the state of the surface Si atoms and oxygen of PSS. For instance, for the bound state $n_i = 2$ and $z_i = -1$, and for the unbound state the $n_i = -2$ and $z_i = 1$.

The σ is defined as:

$$\sigma = \frac{z_i e \theta_i(\varphi)}{A_i} \quad (S5)$$

Where A_i is the saturation density of surface ions and $\theta_i(\varphi)$ is the concentration of the surface ions at a virtual potential (φ) acting on the interface. $\theta_i(\varphi)$ is derived from the Langmuir adsorption isotherm used in interfacial electrochemistry [10] and is defined as:

$$\theta(\varphi) = [1 + (p_{o_2})^{-\frac{1}{n_i}} \exp\left[\frac{\Delta G_i^0 + z_i e \varphi}{k_B T}\right]]^{-1} \quad (S6)$$

Where p_{o_2} is the oxygen partial pressure, k_B is Boltzmann's constant, T is the temperature and ΔG_i^0 is the standard free energy of surface ion formation and correspond to the bound and

unbound states. ΔG_i^0 was determined from the DFT calculated adsorption energies using $\Delta G_i^0 = \frac{E_{Adsorption}}{N_{PSS}}$ where N_{PSS} is the number (16) of silicon atoms in the simulated surface (Figure S1 A).

The polarization P can be shown in the following formula:

$$P = -Z_i e (\theta_i(\varphi) - \theta_0) / A_i \quad (S7)$$

Where θ_0 is introduced to account for the spontaneous formation of Si-O bond between PSS and Si, where σ is non-zero, i.e. when $z_i e \varphi = -\Delta G_i^0$ then $P = 0$ at equilibrium. A_i is the saturation density of surface ions.

Table S1. Numerical values used in our calculations of the Si:PSS interface.

ΔG_+^0	0.13	(eV)	ΔG_-^0	0.08	(eV)
n_+	2		n_-	-2	
z_+	-1		z_-	1	
θ_0	0.5		θ_0	0.5	
T	300	(K)	T	300	(K)
p_{o_2}	1	bar	p_{o_2}	1	bar
A_+	3.0×10^{-19}	(m ²)	A_-	3.0×10^{-19}	(m ²)

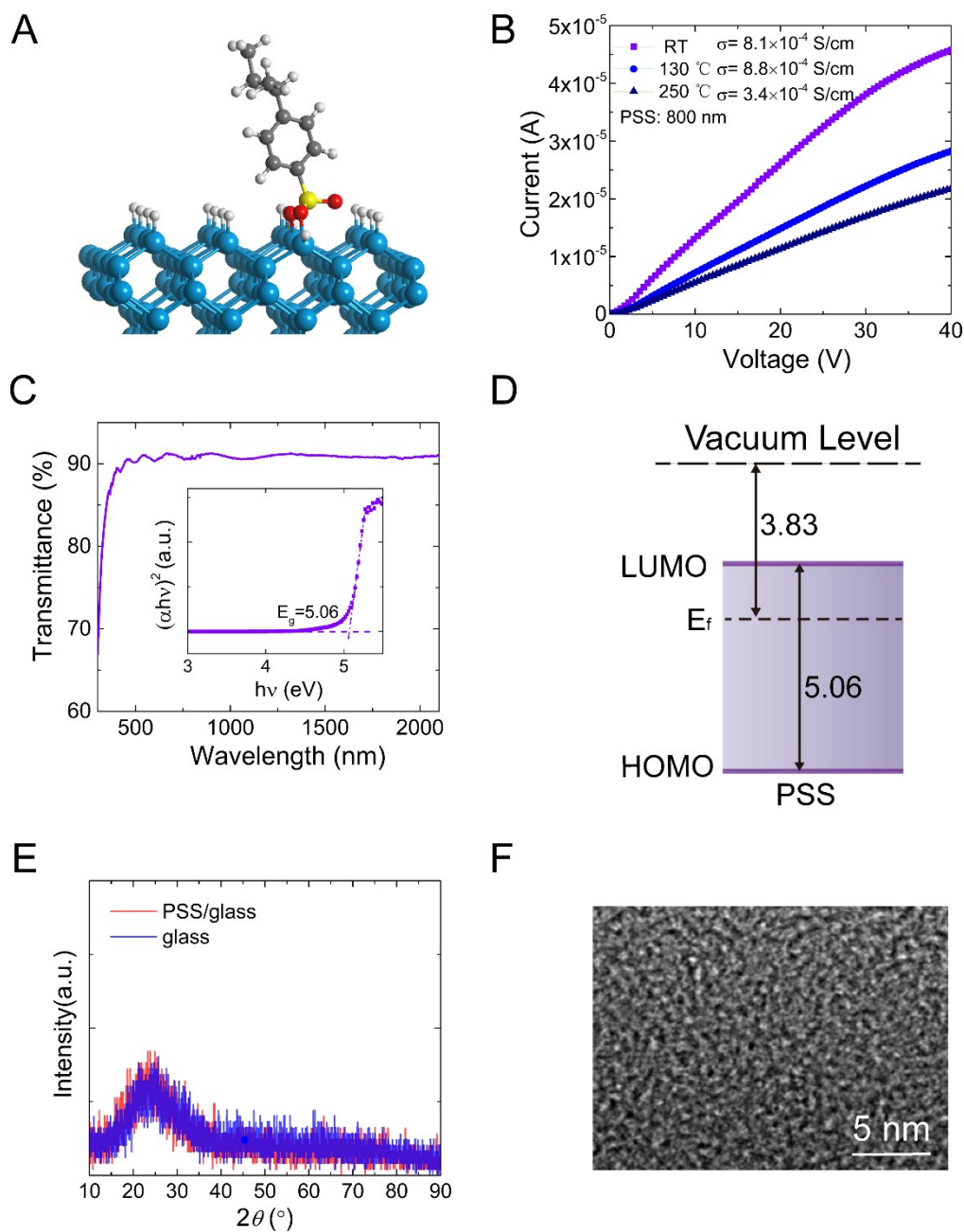


Figure S1 Characteristics of a PSS film. **(A)** Structure of the PSS monomer unit and the H-terminated Si (001) surface from first-principles calculations. **(B)** Conductivity (σ) at the processing temperature of room temperature (RT), 130 °C and 250 °C. The conductivity was measured with a Ag coplanar electrode configuration in the ambient. **(C)** Transmittance with a plot of $(\alpha h\nu)^2$ versus $h\nu$ for the estimation of the optical bandgap (E_g) as an inset. **(D)** Energy level diagram, **(E)** XRD spectra of a film on glass. **(F)** a HRTEM image showing the amorphous structure. In all measurements the PSS film has a thickness of 800 nm.

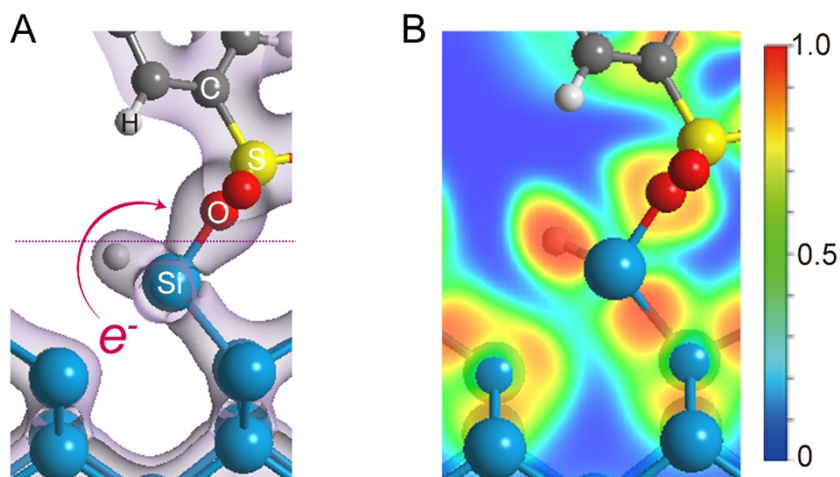


Figure S2. Additional bound state calculations. **(A)** DFT calculated charge density isosurfaces (0.05 e/Bohr^3) for the bound and unbound states and **(B)** the electron localization function. In Fig. 1B, a bound state involving two Si–O bonds is shown. Shown color bar is ELF value. Here, a bound state involving only one Si–O bond is also demonstrated with an adsorption energy of -1.261 eV . This shows that it is possible to have one or two oxygen atoms from one PSS molecule forming bonds with Si on the surface, which is consistent with the experimental results before ^[11]. For example, in our previous work ^[11], XPS data have shown that the interfacial Si has several valence states from Si^{+1} to Si^{+4} , indicating that the Si surface is progressively oxidized by PSS.

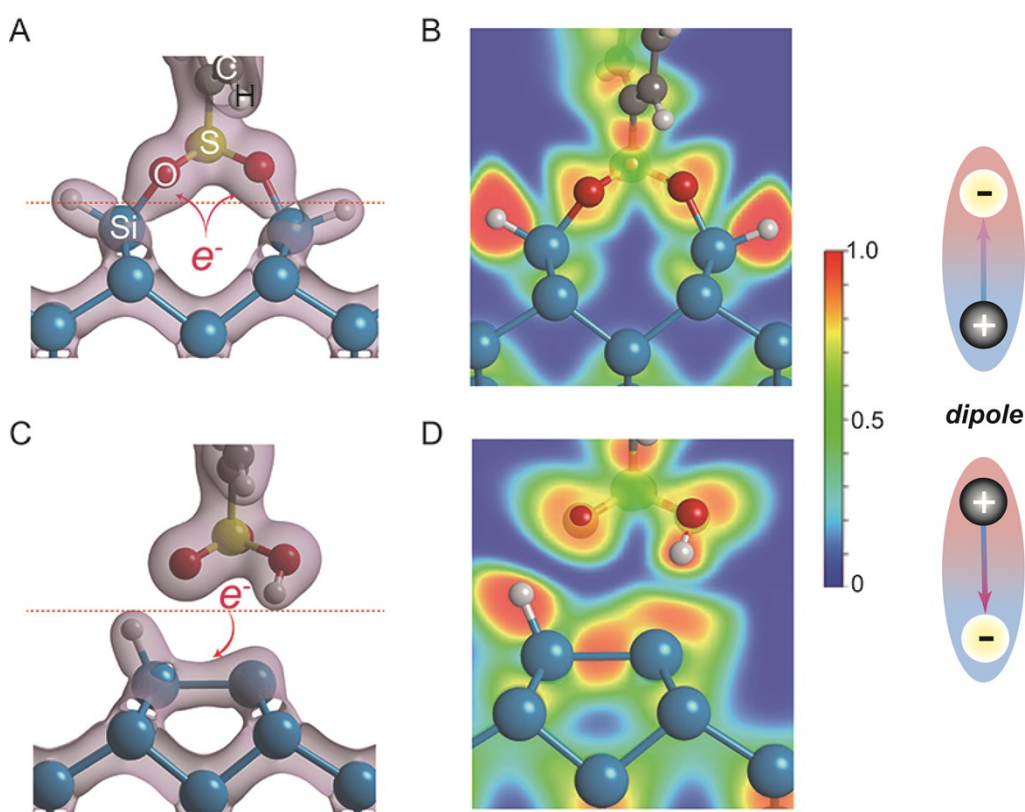


Figure S3. DFT calculations for the interface system exposed to electric fields. **(A)** **(C)** charge density isosurfaces (0.05 e/Bohr^3) and **(B)** **(D)** the electron localization function for positive (top) and negative (bottom) electric fields. In these calculations, the applied bias voltage was simulated by an electrical field of $\pm 0.02 \text{ V/\AA}$ in the *Vienna ab initio Simulation Package* (VASP) and actualized by adding an artificial uniform charge sheets in the vacuum on either side of the slab. As shown, similar charge density and ELF results with those in Figure 1 are obtained. Here, two states correspond to the saturation polarization (P_s) up and P_s down state at a certain voltage bias, with adsorption energies of -2.043 eV and -1.351 eV , respectively, indicating the existence of a bistable electrical polarization.

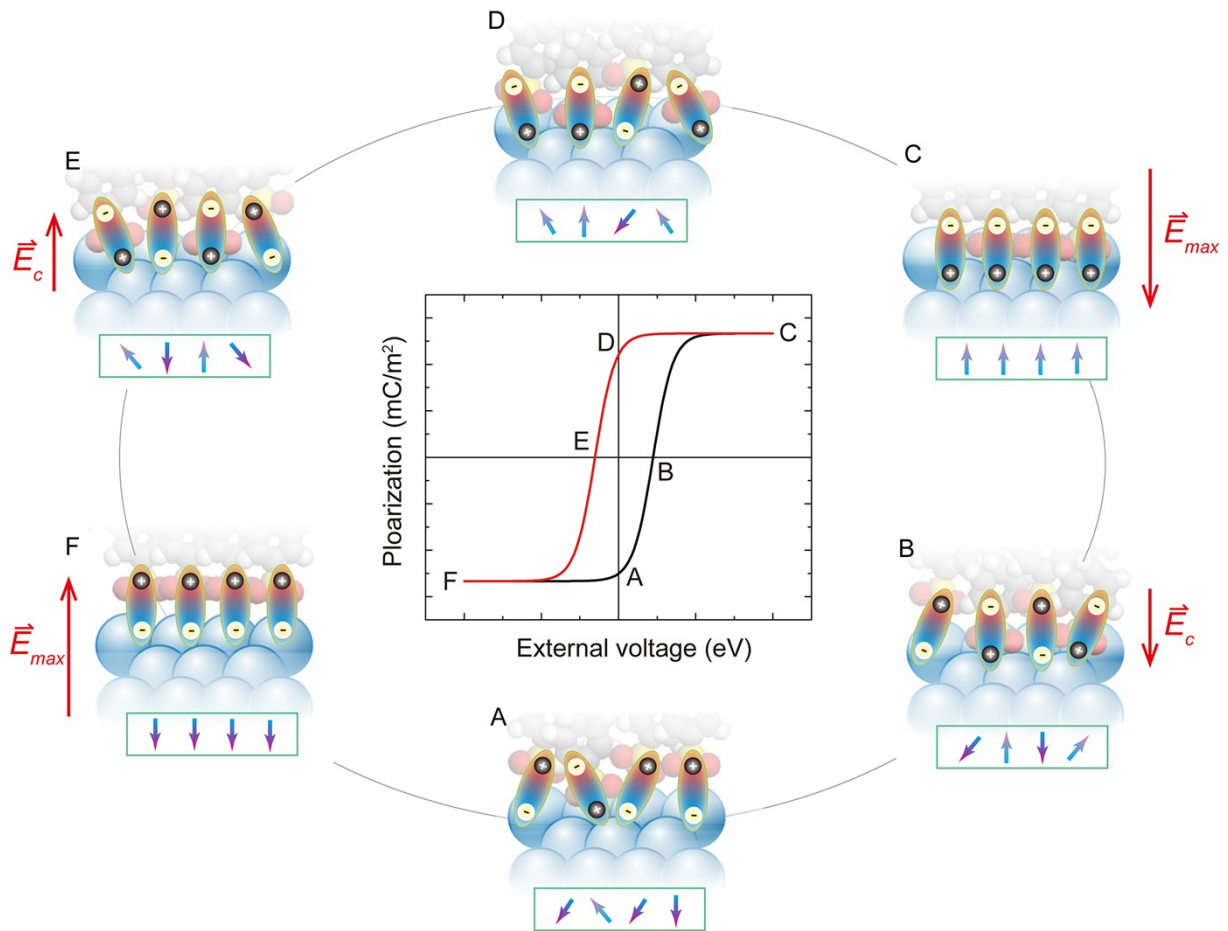


Figure S4. Mechanism of interfacial ferroelectricity. Several critical points including remnant polarization, coercive field and saturation polarization. The arrows show the polarization of SIDs and their direction. The total polarization is the vector sum of all arrows in a green interface box.

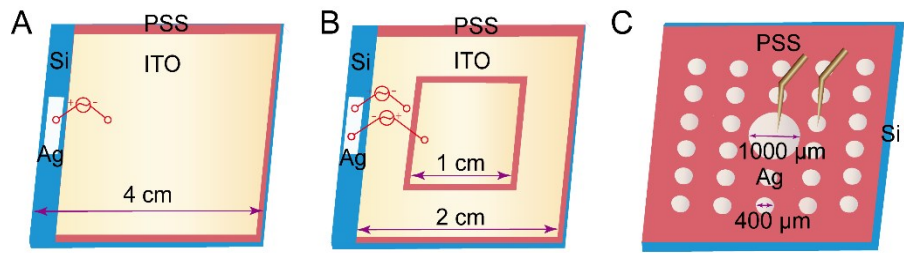


Figure S5. Geometry of the metal-insulator-semiconductor capacitor used for characterization. **(A)** For TEM and interface recombination velocity; **(B)** For PL; **(C)** For ferroelectric properties. A 200-nm-thick silver pad is evaporated through a shadow mask on top of the PSS.

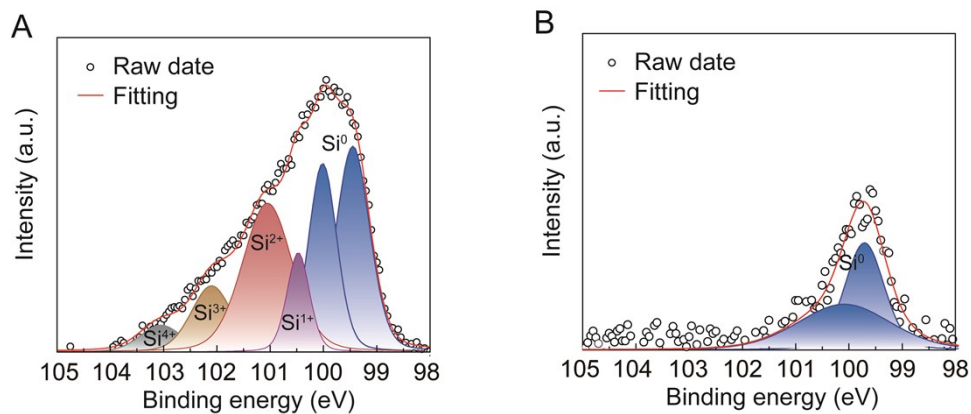


Figure S6. Si 2p XPS for interface characterization. **(A)** P_r up; **(B)** P_r down. The signal is deconvoluted to several valence states (from Si¹⁺ to Si⁴⁺) of Si atoms bonded to oxygen atoms, which are detected aside from the Si species (Si⁰) located at 99.3–99.8 eV. The detailed method can be seen elsewhere ^[12-15] and Si valence state data also can be checked on the National Institute of Standards and Technology (NIST) Standard Reference Database ^[16].

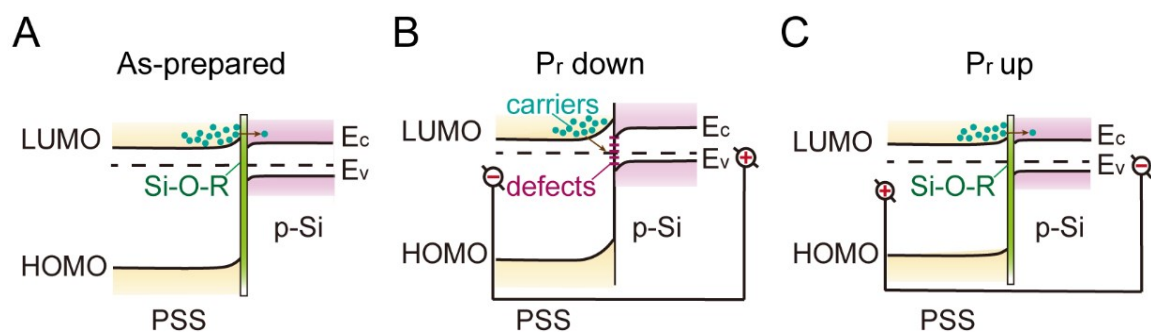


Figure S7. Band alignment diagram of interface between PSS and Si. **(A)** As prepared and without any voltage biasing. The interface is in the bound state due to the spontaneous polarization. **(B)** A negative voltage is applied to obtain the P_r down state **(C)** A positive voltage is applied to obtain the P_r up state. P_r up and down states are induced by external voltage bias to local on bound and unbound state, respectively.

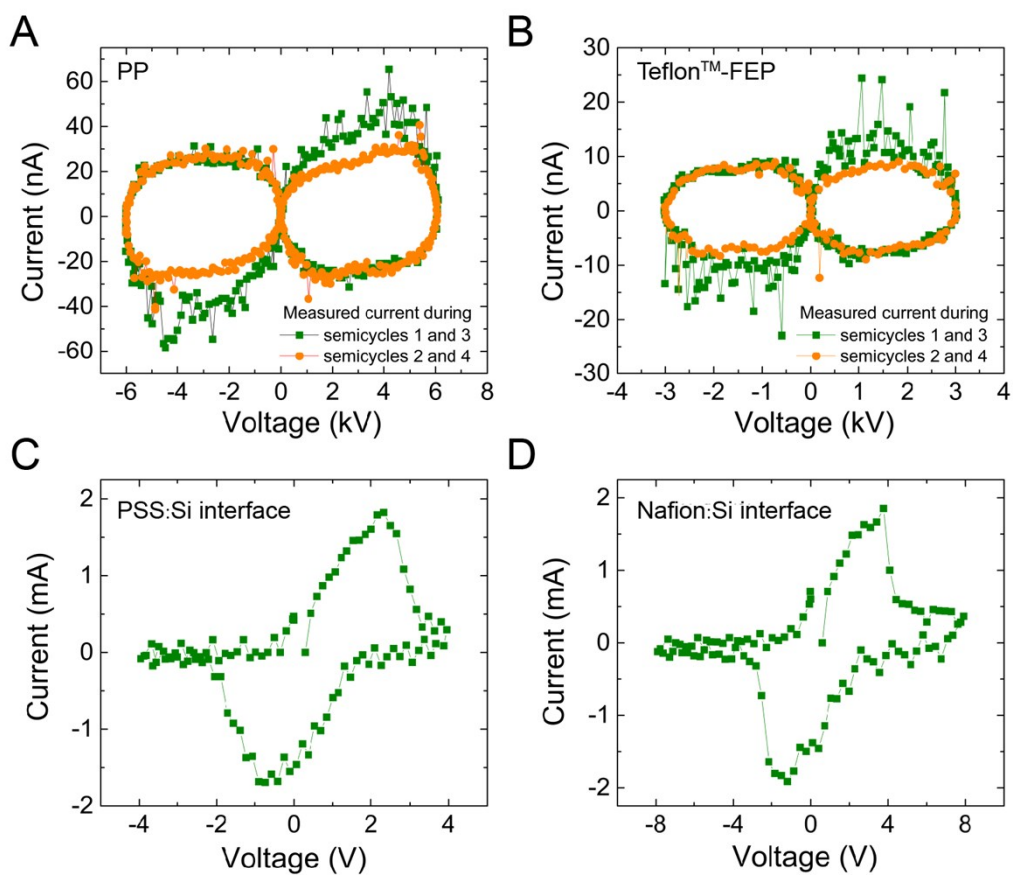


Figure S8. Charging currents. (A) a cellular polypropylene (PP) ferroelectret film (B) a Teflon™-FEP tubular-channel ferroelectret system. Note that here data come from the reference^[17]. (C) the Ag/PSS/Si and Ag/Nafion/Si organic-inorganic hybrid interface ferroelectric capacitor. Nafion has the same sulfonic functional group $-\text{SO}_3\text{H}$ (see Figure S15).

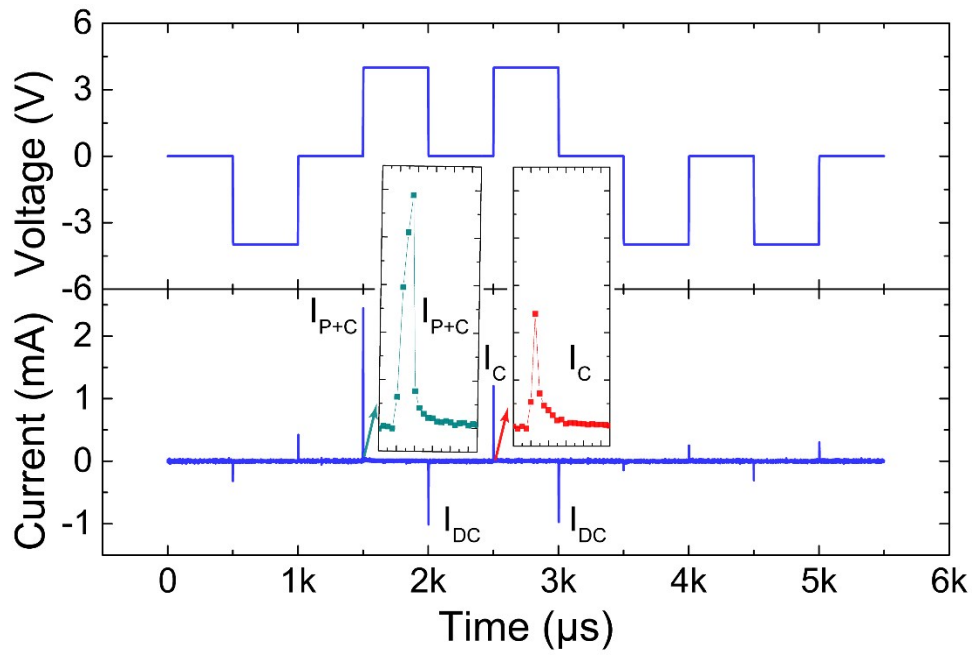


Figure S9. Double pulse measurement diagram. I_{P+C} is the polarization switching current plus the capacitor charging current, I_C is the capacitor charging current, I_{DC} is the capacitor discharge current. The polarization switching current (I_P) can be estimated from the difference between I_{P+C} and I_C . An enlargement of I_{P+C} and I_C are shown as an inset.

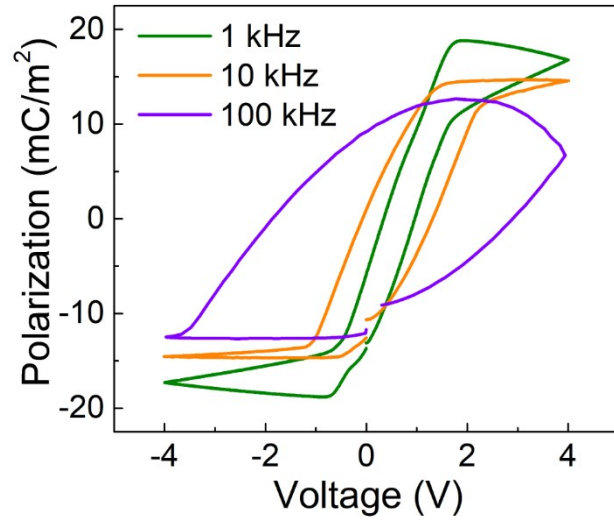


Figure S10. P-V hysteresis loops with different frequencies for Ag/PSS/Si capacitors with 800 nm-thick PSS thin film.

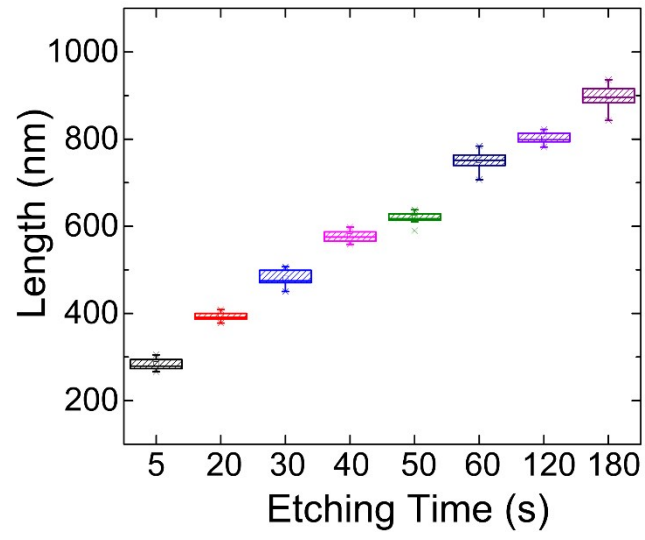


Figure S11. Length of the obtained silicon nanowires in black silicon with etching time.

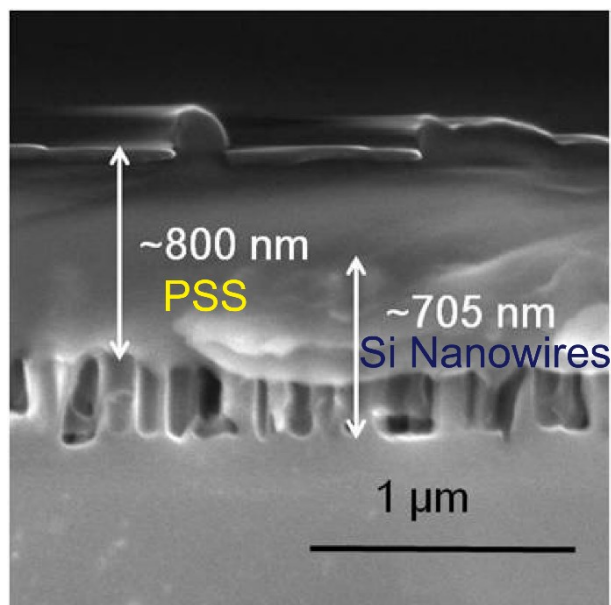


Figure S12. SEM image of PSS on black silicon. The thickness of PSS is ~ 800 nm and the length of Si nanowires is ~ 705 nm. The PSS is unable to infiltrate the entire length of the silicon nanopore.

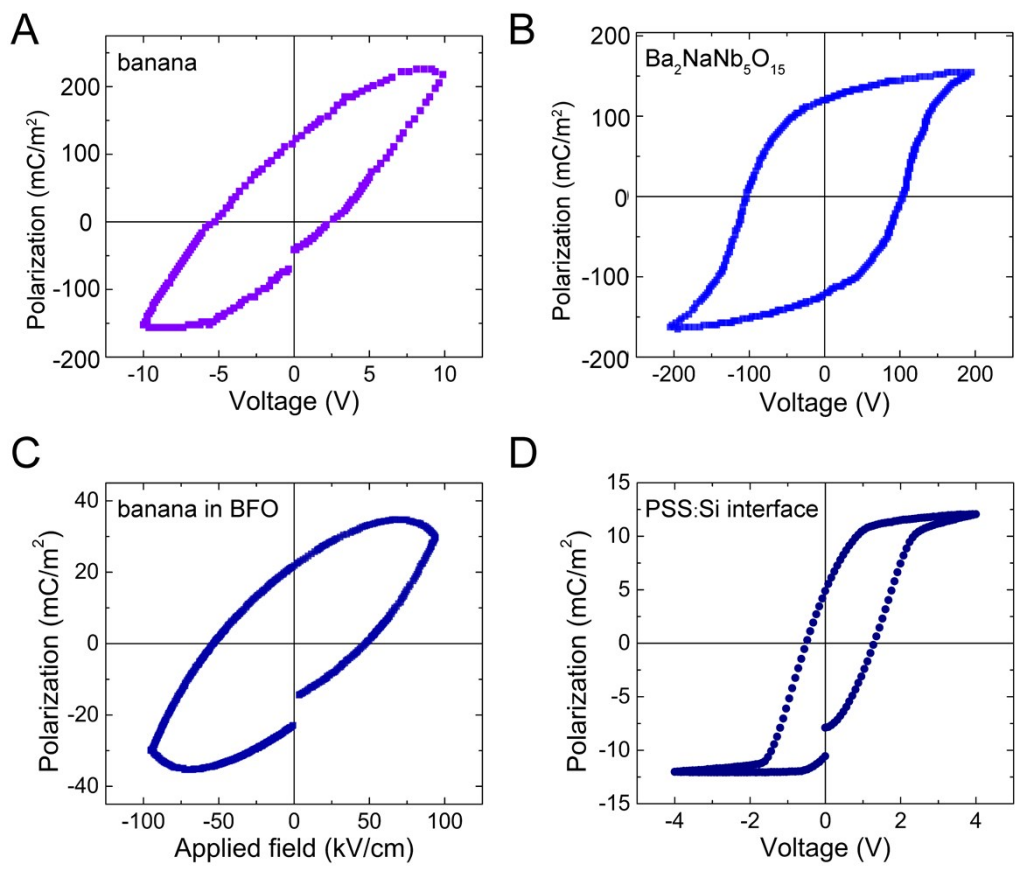


Figure S13. P-V hysteresis loops for different ferroelectrics **(A)** banana^[18]. **(B)** The ferroelectric material Ba₂NaNb₅O₁₅^[18]. **(C)** banana in BiFeO₃ (BFO)^[19]. **(D)** PSS:Si interface.

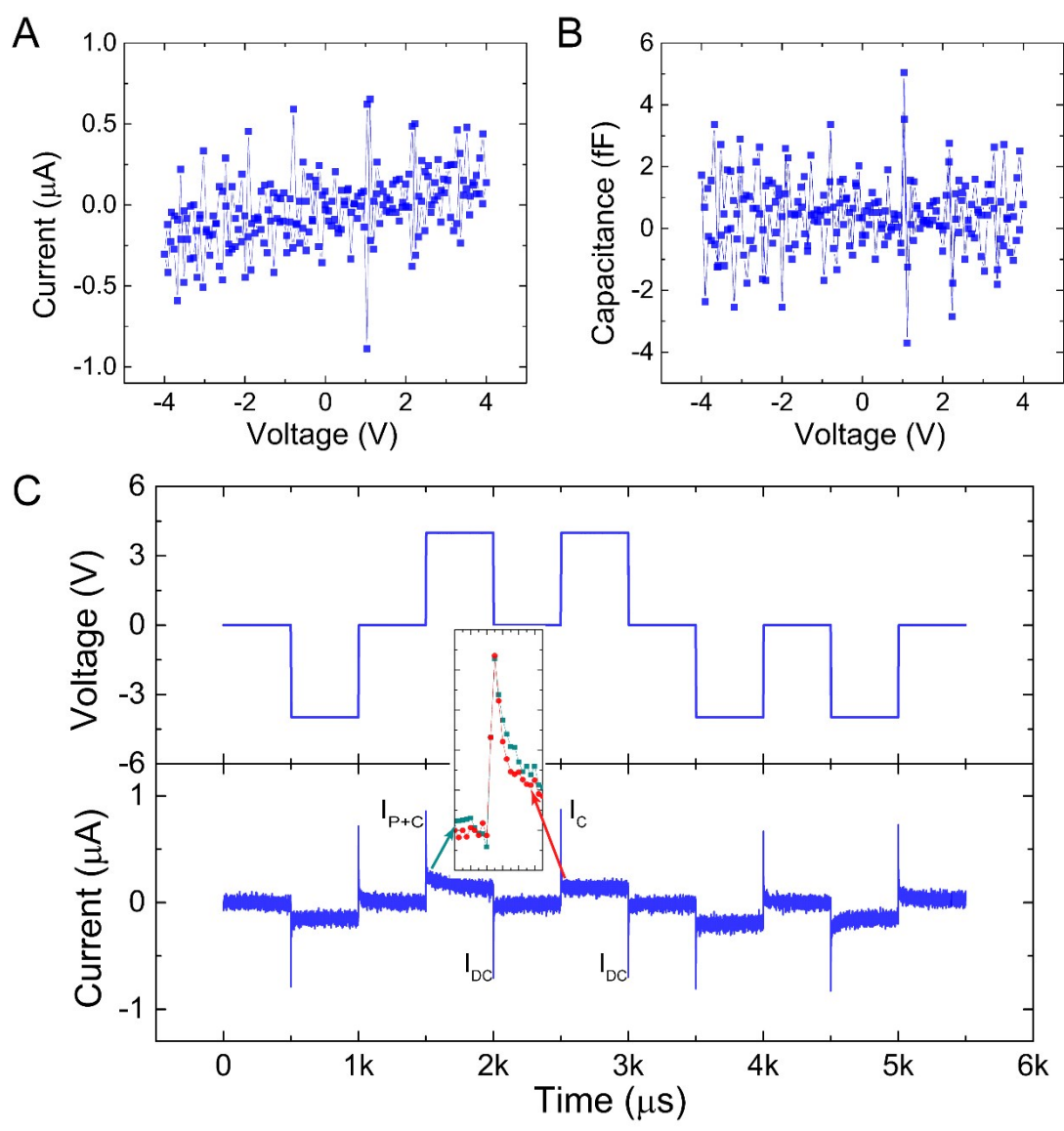


Figure S14. The electrical performance of Ag/PSS/Pt capacitor. **(A)** Current-voltage; **(B)** Capacitance-voltage; **(C)** Double pulse measurement diagram. I_{P+C} is the polarization switching current plus the capacitor charging current, I_C is the capacitor charging current, I_{DC} is the capacitor discharge current. The polarization switching current (I_P) can be estimated from the difference between I_{P+C} and I_C . An enlargement of I_{P+C} and I_C are shown as an inset.

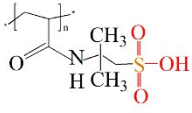
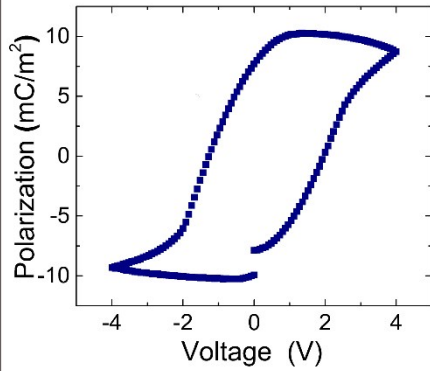
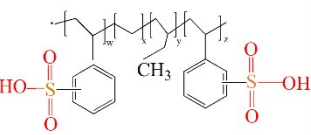
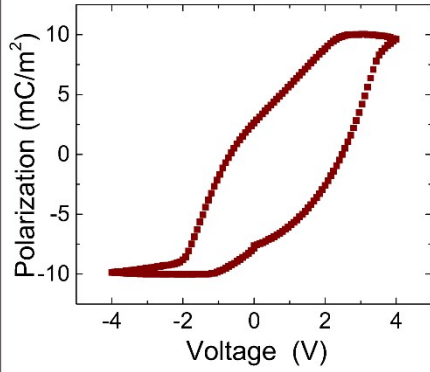
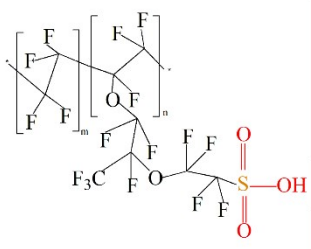
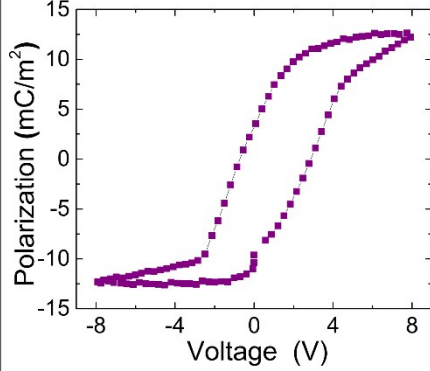
Material	Molecular Formula	Conductivity (S/cm)	P-V Hysteresis Loop
PAMPS		$(1.0-1.2) \times 10^{-4}$	
PS-b-PERB		$(2.7-23.1) \times 10^{-6}$	
Nafion		$(2.9-27.6) \times 10^{-7}$	

Figure S15. P-V hysteresis loops for other materials with a $-\text{SO}_3\text{H}$ group interfaced with silicon: poly(2-acrylamido-2-methylpropanesulfonic acid) (PAMPS), polystyrene-block-poly(ethylene-ran-butylene)-block-polystyrene, sulfonated, cross-linkable (PS-b-PERB) and Nafion. The thickness of the films are 600 nm, 290 nm, 2.5 μm , respectively. The conductivity and molecular formula are displayed.

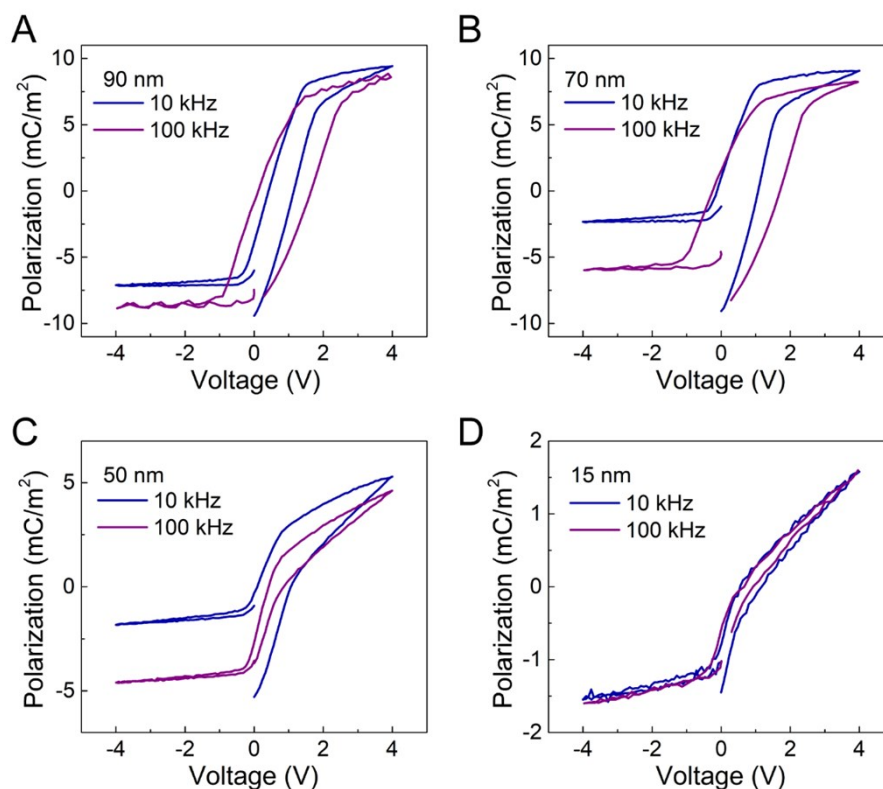


Figure S16. P-V hysteresis loops for Ag/PSS/Si capacitors with different thickness of PSS. (A) 90 nm (B) 70 nm (C) 50 nm (D) 15 nm. Here note that the starting point and the ending point of the hysteresis loops are in the opposite position. In technology, this is caused by water invasion, too thin thickness and/or bad top electrode. It is speculated that the unstable contact resistance between top Ag electrode and PSS surface cause a potential conductive fuse in the system and/or screening of the dipoles.

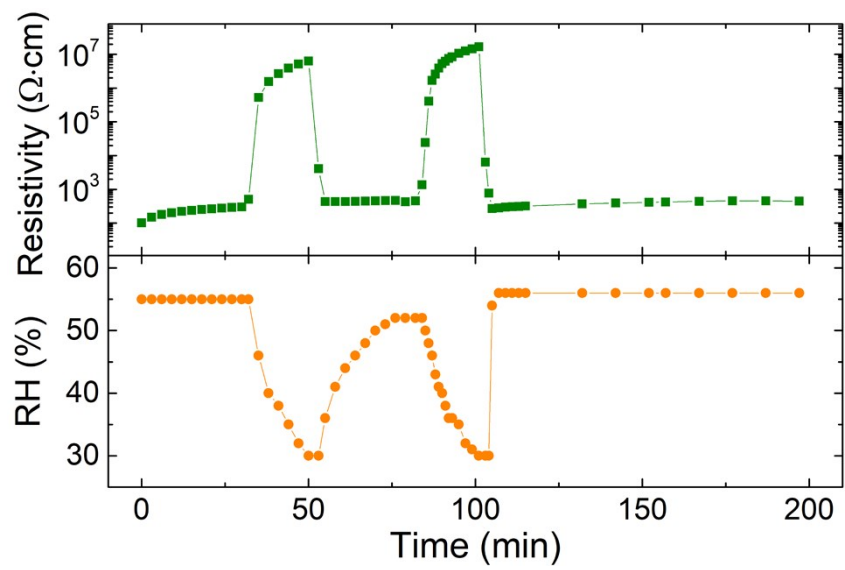


Figure S17 The PSS resistivity changed as environment humidity.

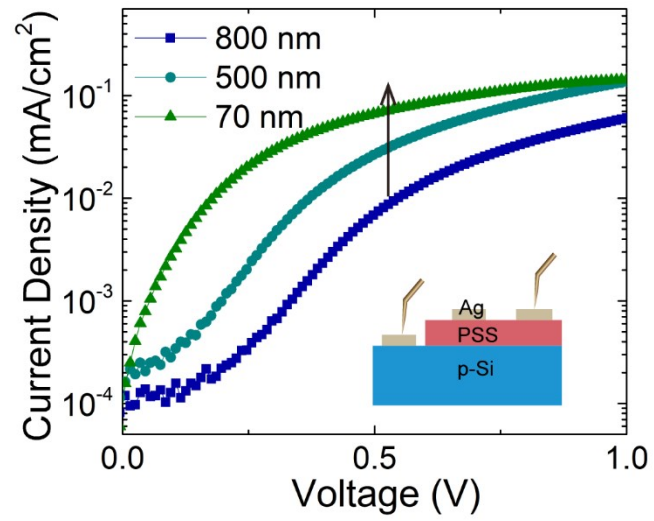


Figure S18. An I-V measurement of Ag/PSS/Si capacitor with different PSS thicknesses.

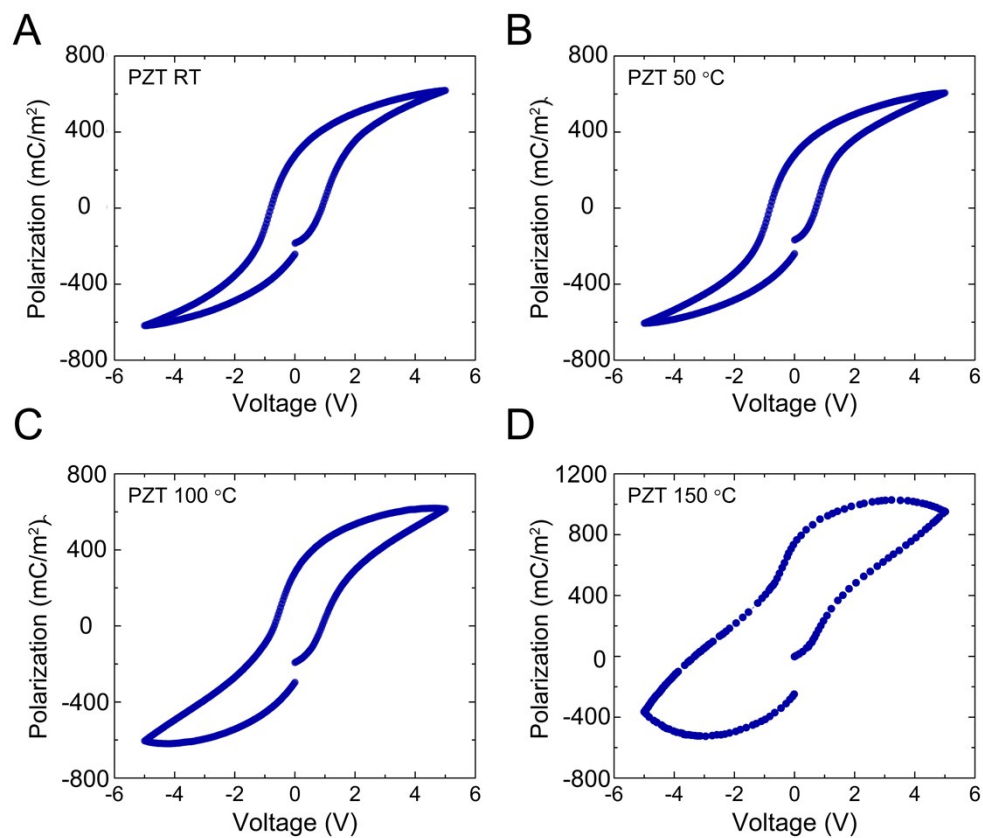


Figure S19. P-V hysteresis loops for devices fabricated from lead zirconate titanate (PZT) at different temperatures **(A)** RT **(B)** 50 °C **(C)** 100 °C **(D)** 150 °C.

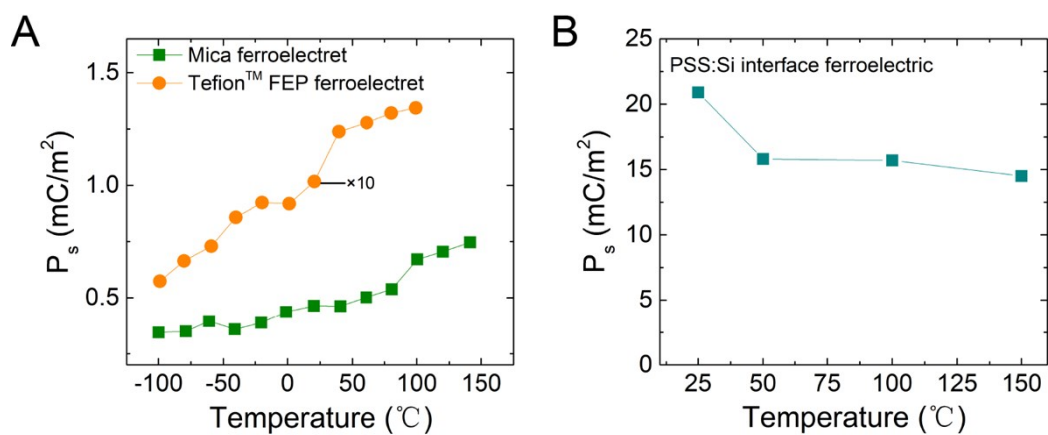


Figure S20. The saturated polarization (P_s) as function of test temperature. **(A)** Teflon™ fluoroethylenepropylene (FEP) copolymer ferroelectret^[20] and mica electrets^[21] **(B)** PSS/Si interface ferroelectric capacitor.

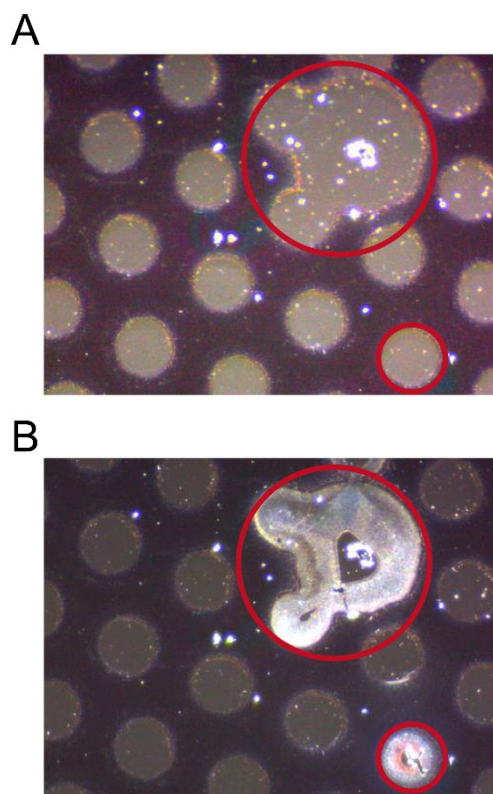


Figure S21. Microscope images of the Ag disk electrode **(A)** Before the fatigue test **(B)** After the fatigue test. Red circles indicate the pads used to connect the capacitor device.

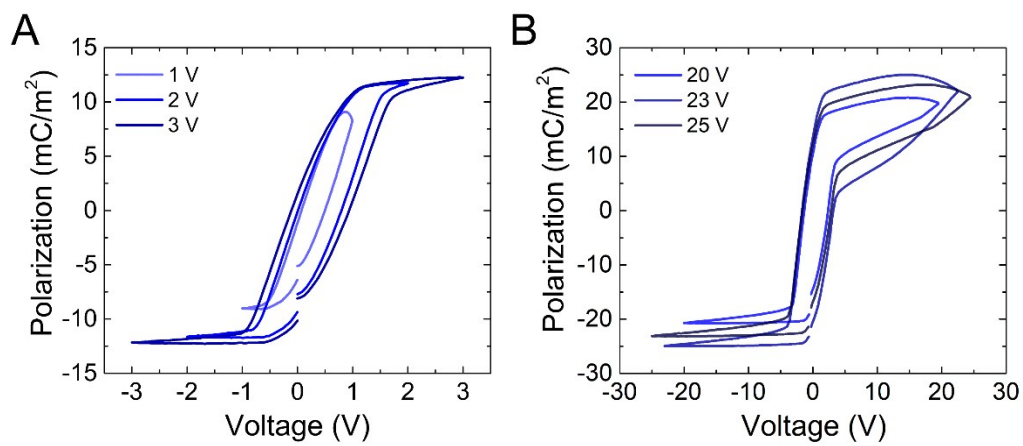


Figure S22. Ferroelectric polarization hysteresis loops at different voltages. **(A)** Low voltage of 1-3 V. **(B)** High voltage of 20-25 V.

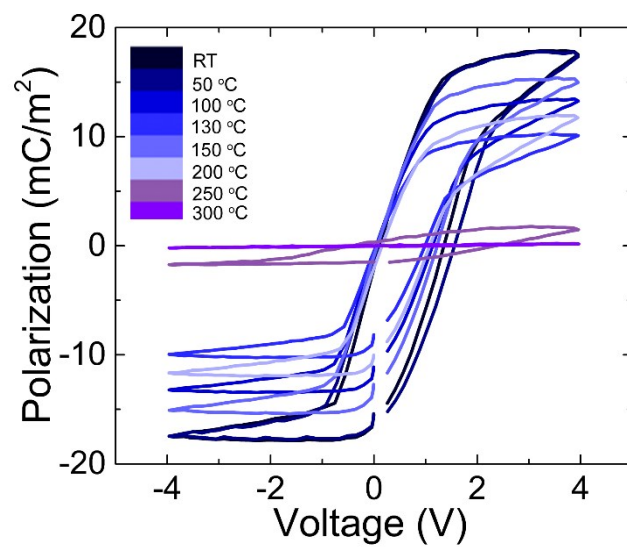


Figure S23. P-V curves of the device with different processing temperatures of the PSS thin film.

References

- [1] Z. Huang, N. Geyer, P. Werner, J. de Boor, U. Gosele, *Advanced materials* **2011**, 23, 285.
- [2] G. Kresse, J. Hafner, *Physical Review B* **1993**, 47, 558.
- [3] G. Kresse, J. Furthmüller, *Computational materials science* **1996**, 6, 15.
- [4] J. P. Perdew, K. Burke, M. Ernzerhof, *Phys. Rev. Lett.* **1996**, 77, 3865.
- [5] P. E. Blöchl, *Physical review B* **1994**, 50, 17953.
- [6] C. Elsässer, M. Fähnle, C. Chan, K. Ho, *Physical Review B* **1994**, 49, 13975.
- [7] S. Grimme, J. Antony, S. Ehrlich, H. Krieg, *The Journal of chemical physics* **2010**, 132, 154104.
- [8] S. Grimme, S. Ehrlich, L. Goerigk, *J. Comput. Chem.* **2011**, 32, 1456.
- [9] M. J. Highland, T. T. Fister, D. D. Fong, P. H. Fuoss, C. Thompson, J. A. Eastman, S. K. Streiffer, G. B. Stephenson, *Physical review letters* **2011**, 107, 187602.
- [10] S. M. Yang, A. N. Morozovska, R. Kumar, E. A. Eliseev, Y. Cao, L. Mazet, N. Balke, S. Jesse, R. K. Vasudevan, C. Dubourdieu, S. V. Kalinin, *Nature Physics* **2017**, 13, 812.
- [11] J. Chen, Y. Shen, J. Guo, B. Chen, J. Fan, F. Li, H. Liu, Y. Xu, Y. Mai, *Applied Physics Letters* **2017**, 110, 083904.
- [12] J. Chen, Y. Shen, J. Guo, B. Chen, J. Fan, F. Li, B. Liu, H. Liu, Y. Xu, Y. Mai, *Electrochimica Acta* **2017**, 247, 826.
- [13] K. Roodenko, F. Yang, R. Hunger, N. Esser, K. Hinrichs, J. Rappich, *Surface Science* **2010**, 604, 1623.
- [14] C. Gondek, M. Lippold, I. Röver, K. Bohmhammel, and E. Kroke, *J. Phys. Chem. C* **2014**, 118, 2044.
- [15] G. Cerofolini, A. Giussani, A. Modelli, D. Mascolo, D. Ruggiero, D. Narducci, E. Romano, *Applied Surface Science* **2008**, 254, 5781.
- [16] <http://dx.doi.org/10.18434/T4T88K>.
- [17] X. Qiu, L. Holländer, W. Wirges, R. Gerhard, H. Cury Basso, *Journal of Applied Physics* **2013**, 113, 224106.
- [18] J. F. Scott, *Journal of Physics: Condensed Matter* **2008**, 20, 021001.
- [19] A. K. Pradhan, K. Zhang, D. Hunter, J. B. Dadson, G. B. Loitts, P. Bhattacharya, R. Katiyar, J. Zhang, D. J. Sellmyer, U. N. Roy, Y. Cui, A. Burger, *Journal of Applied Physics* **2005**, 97, 093903.
- [20] X. Qiu, W. Wirges, R. Gerhard, *Applied Physics Letters* **2016**, 108, 252901.
- [21] X. Qiu, M. Steffen, W. Wirges, R. Gerhard, "Temperature dependence of quasi-ferroelectric hysteresis in a model ferroelectret system", presented at *2015 IEEE Conference on Electrical Insulation and Dielectric Phenomena (CEIDP)*, 2015.